Protein Science (1999), *8*:2281–2289. Cambridge University Press. Printed in the USA.

Molecular dynamics investigation of the effect of an antiviral compound on human rhinovirus

DONALD K. PHELPS[1] AND CAROL BETH POST

Department of Medicinal Chemistry, Purdue University, West Lafayette, Indiana 47907-1333

(RECEIVED February 11, 1999; ACCEPTED July 23, 1999)

Abstract

The factors that influence the enhanced stability observed experimentally of human rhinovirus 14 (HRV14) upon binding a hydrophobic antiviral drug have been investigated by molecular dynamics. Simulations centered about the HRV14 drug-binding pocket allow the reliable assessment of differences in capsid protein motions of HRV14 and drug-bound HRV14. We propose that the experimentally observed stabilization of the ligated virus arises from higher entropy, rather than enthalpy. Time-averaged interaction energies between the viral protein and molecules occupying the pocket are less favorable in the presence of the drug, consistent with the proposal that the observed stability arises from entropic effects. Interaction energies characterizing subunit–subunit contacts within one viral protomer are found to be substantially stronger than those between two protomers. Such distinction in subunit interaction would have clear implications on assembly and disassembly. Drug binding is found to affect large-scale, collective properties, while leaving local atomic properties unperturbed. Specifically, the simulations reveal a weakening of long-range correlations in atomic motions upon drug binding. On the other hand, neither the fast time scale RMS fluctuations of individual atomic positions nor the fluctuation build-up curves from the capsid β-sandwich forming the drug-binding pocket show a consistent distinction between the drug-bound and drug-free viral simulations. Collectively, the detailed description available from the simulations provides an understanding of the experimental observations on the drug-induced changes in thermal stability and protease sensitivity reported for picornaviruses. The predicted significance of binding entropy can be explored experimentally and should be considered in the design of new antiviral compounds.

Keywords: antiviral; molecular dynamics; protein stability, rhinovirus; stochastic boundary

The WIN family of hydrophobic antipicornaviral drugs is effective against human rhinovirus (HRV), the cause of the common cold. The antiviral mechanism of these drugs is of interest to provide a rational basis for the design of new antiviral drugs. These drugs bind to an internal cavity or pocket of HRV, which is naturally occupied by either water molecules (Rossmann et al., 1985) or perhaps by a long chain molecule of unknown identity, which is seen in the crystal structures of picornaviruses (Filman et al., 1989; Rossmann, 1994). It is known that many members of this family of drugs prevent uncoating and stabilize against transition of HRV to a noninfectious virus particle at high temperatures (Fox et al., 1986; Rombaut et al., 1991; Bibler-Muckelbauer et al., 1994), or at low pH (Heinz et al., 1990). We have suggested the basis for antiviral activity by the WIN-type compounds is entropic stabilization of HRV14 (Phelps & Post, 1995; Phelps et al., 1998).

Reprint requests to: Carol Beth Post, Department of Medicinal Chemistry, Purdue University, West Lafayette, Indiana 47907-1333; e-mail: cbp@cc.purdue.edu.

[1]Current address: Air Force Research Laboratory, AFRL/PRSF Bldg. 490, 1790 Loop Rd. N., Wright-Patterson AFB, Ohio 45433.

Crystallographic studies reveal that HRV14 is an icosahedral virus comprising 60 copies of four viral polypeptides VP1, VP2, VP3, and VP4 (Fig. 1). A deep canyon surrounds each fivefold axis, and the base of the canyon covers the drug-binding pockets that are located primarily within the β-sandwiches of VP1. Poliovirus (Filman et al., 1989) and other picornaviruses have similar pockets suggesting a functional role of the pocket in the viral life cycle (Smith et al., 1986; Grant et al., 1994). In fact, certain thermolabile mutants require drug molecules for stability in the extracellular environment, and without the drug these virions lose VP4 and become noninfectious (Grant et al., 1994).

The stabilization of rhinovirus by WIN compounds is examined here by probing the detailed molecular motions by the method of molecular dynamics. The antiviral drug WIN52084s (Fig. 2) and the virus HRV14 have been chosen for this study due to the availability of refined atomic-resolution crystal coordinates for both HRV14 (Rossmann et al., 1985) (Protein Data Bank (PDB) entry 4rhv, 3.0 Å resolution) and drug-bound HRV14·WIN52084s (PDB entry 2rsl, 3.0 Å resolution) (Smith et al., 1986). Analysis of the enormous quantity of information from the simulations of these systems has identified properties that reflect the influence of the bound drug, thus gaining insight into antiviral activity. Trajectories

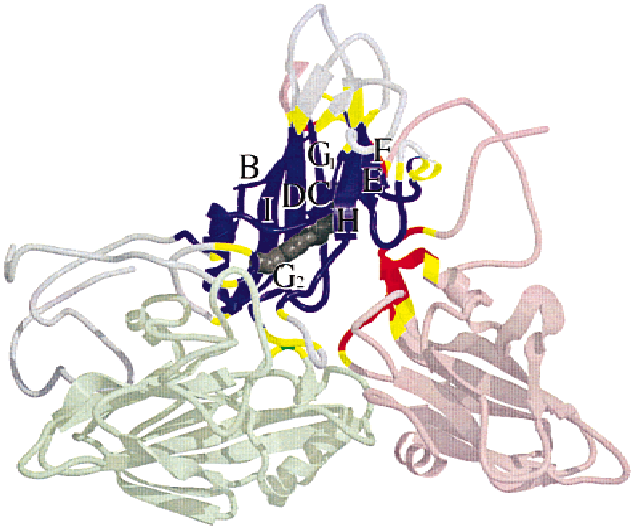

Fig. 1. A Raster3D (Merritt & Bacon, 1997) ribbon created with a MOLSCRIPT generated input file (Kraulis, 1991) of VP1, VP2, and VP3b. The central darker colored region represents the SBMD simulation sphere. Colors indicate: yellow = harmonically constrained region; blue = VP1; green = VP2; red = VP3b; grey spheres = WIN52084s; lighter blue, green and red ribbons = exterior to SMBD sphere. A small number of residues from neighboring subunits and VP4 are included in the calculations but are not shown in figure.

of 800 ps were calculated for a reduced system of the virus particle with 3,000 atoms. Three different solvation boundary conditions were employed to ensure that differences in the solvation model are not responsible for differences in dynamics between HRV14 and HRV14·WIN52084s. In addition, calculations have been performed on a theoretical "polar" WIN molecule to distinguish dynamical and energetic effects related specifically to WIN52084s and to structural changes in VP1m, which occur due to displacement of residues by WIN.

Earlier studies (Phelps & Post, 1995; Phelps et al., 1998) on HRV14 and HRV14·WIN52084s reveal two properties of the virus capsid, which differ as a result of WIN52084s binding. The difference was attributed to the hydrophobic nature of WIN52084s. Antiviral binding causes an increase in the compressibility of the drug-free virion (Phelps & Post, 1995). Consideration of the dependence observed in experimental compressibilities on the unfolding entropies of globular proteins led to the conclusion that the calculated change in compressibility of the virus indicates that drug binding enhances stability by increasing the conformational entropy of the virus. In addition to the change in compressibility, the earlier studies found differences in free volume and the thermal expansivity of the two systems (Phelps et al., 1998) and the temperature dependence of their mobility, effects that can be considered an alternative reflection of the change in conformational entropy described earlier (Phelps & Post, 1995). (Free volume is defined to be that volume within the molecular volume and outside of the van der Waals radii of any atom.)

In this paper, we present results that reveal that binding of the antiviral compound does indeed confer a more hydrophobic nature to the viral system. Increased hydrophobicity, associated with weaker intermolecular forces in the viral pocket upon drug binding, is evidenced by weaker positional correlations between protein Cαs for HRV14·WIN52084s than for HRV14. That is, the change in hydrophobic nature also affects long-range correlations in atomic motions. Calculations of interaction energies between various viral proteins, water molecules, and WIN52084s are a direct measure of the hydrophobic nature. The internal energy of the viral complex is indeed less favorable when WIN25084s is bound, consistent with drug stabilization of HRV14 primarily by entropic means. We also compare RMS fluctuations of HRV14 and HRV14·WIN52084s with appropriately scaled crystallographic *B*-values. Interestingly, analysis of the motions of residues near the drug-binding pocket reveal a potential drug entry site consistent with the visual interpretation for the pocket opening (Kim et al., 1993).

Materials and methods

The stochastic boundary molecular dynamics (SBMD) method is applied to the capsid proteins of human rhinovirus 14 (HRV14) with and without an antiviral drug bound to an internal cavity (or pocket) at the base of a deep canyon in the virus surface. The SBMD method is applied as described in detail by Brooks and Karplus (1983). A brief summary of the method and details specific to this study are given below.

The simulations were carried out using the CHARMM macromolecular mechanics program (Brooks et al., 1983) version 22 and the CHARMM version 19 polar hydrogen parameter set. This parameterization includes only hydrogens that can form hydrogen bonds explicitly, while other hydrogens are implicitly modeled as extended heavy atoms. Additional parameters necessary to model WIN52084s are from Lybrand and McCammon (1988). A theoretical "polar" WIN, pWIN52084s has parameters identical to WIN52084s except for charges as given in Table 1. Water is represented by the TIP3 model. Hydrogen–oxygen bonds in water and explicit hydrogen–heavy protein atom bonds are fixed using SHAKE (Ryckaert et al., 1977).

The system is spatially subdivided into reaction, buffer, and reservoir regions. The reaction region of specific interest is a 20 Å radius sphere centered about the drug-binding pocket, and where molecular dynamics (MD) determines the atomic trajectories. In Figure 1, the main chain in the MD region is colored either darker blue (VP1), green (VP2), or red (VP3). The buffer region, a spherical shell ranging 20 to 22 Å from the center of the reaction region

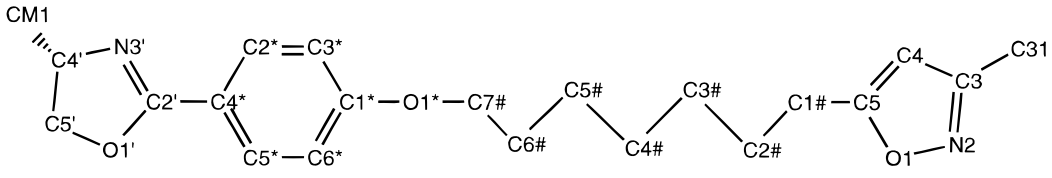

Fig. 2. Structure of WIN52084s. See Table 1 for information on atom labels.

Table 1. *Atomic charges for WIN52084s and pWIN52084s*

WIN52084s[a]			pWIN52084s
Atom name[b]	Atom type	Charge	Charge
O1	OW	−0.11	−0.11
N2	NR	−0.49	−0.49
C3	CC	0.78	0.78
C4	CR1E	−0.54	−0.54
C31	CH3E	−0.15	−0.15
C5	CS	0.55	0.55
C1#	CH2E	−0.01	−0.51
C2#	CH2E	0.00	0.50
C3#	CH2E	0.00	−0.50
C4#	CH2E	0.00	0.50
C5#	CH2E	0.00	−0.50
C6#	CH2E	0.00	0.50
C7#	CH2E	0.16	0.16
O1*	OW	−0.37	−0.37
C1*	CJ	0.46	0.46
C2*	CR1E	−0.16	−0.66
C3*	CR1E	0.18	0.68
C4*	CJ	−0.50	−0.50
C5*	CR1E	0.18	0.68
C6*	CR1E	−0.16	−0.66
N3′	NR	−0.67	−0.67
C2′	CV	0.83	0.83
O1′	OW	−0.42	−0.42
C5′	CH2E	0.13	0.13
C4′	CH1E	0.46	0.46
CM1	CH3E	−0.15	−0.15

[a] From Lybrand and McCammon (1988).
[b] See Figure 2 for structure.

and colored yellow in Figure 1, acts as a shield between the reaction and reservoir regions. Buffer atom motions are obtained by Langevin dynamics (LD). Reservoir region atoms (lighter shades of blue, red, and green in Fig. 1) are removed, and their influence on the system is mimicked by stochastic forces applied to the buffer (or Langevin) atoms. Harmonic restoring forces constrain protein atoms in the buffer region (see Table 2) to positions centered about their X-ray coordinates and help maintain the structural integrity of the system. The X-ray structure was overlayed with water molecules to eliminate water-sized holes in the simulation sphere. A deformable stochastic boundary (Brooks & Karplus, 1983), which applies a rapidly increasing force beyond the boundary radius, maintains water molecules within the simulation sphere.

Rules specifying the partitioning of atoms or residues between the MD, buffer, and reservoir regions differ somewhat from the original implementation (Brooks & Karplus, 1983) and apply as follows:

1. Side-chain atoms are included in the reaction (or MD) region if at least one atom in the side chain is <20 Å from the center of the simulation sphere.
2. All main-chain atoms that are less than 20 Å from the center of the simulation sphere are in the MD region.
3. If an entire residue is outside of a 22 Å radius, then it is deleted unless the inclusion of one to three residues provides continuity of the protein backbone.
4. Atoms greater than 20 Å from the center use Langevin dynamics except as excluded by rule 1.
5. Buffer region (LD region) protein atoms are loosely fixed about X-ray coordinates by harmonic constraints.

Table 2. *Stochastic boundary force parameters (Brooks & Karplus, 1989)*

Atom type	Inverse mean-squared fluctuations ($Å^{-2}$)	Langevin friction coefficient (ps^{-1})
Main chain	2.44	80
Side chain	1.37	80
Sulfur	3.28	80

Harmonic constraints differ according to the atom type (see Table 2) and are scaled by $S(r_i)$

$$S(r_i) = \begin{cases} 0 & R_1 \le |r_i| \\ \frac{1}{2}\,\frac{(r_i - R_1)^2(3R_2 - R_1 - 2r_i)}{(R_2 - R_1)^3} & R_1 < |r_i| \le R_2 \\ 0.5 & |r_i| > R_2 \end{cases}$$

where $R_1 = 20$ Å, $R_2 = 22$ Å, and r_i is the distance of atom i from the center of the simulation sphere. Friction coefficients for protein heavy atoms and water oxygen atoms in the LD region are also scaled with $S(r_i)$. A 22 Å radius sphere is large enough that boundary atoms are identical for HRV14 and HRV14·IN52084s systems. This allows the systems to be set up with exactly the same protein atoms and harmonic constraints.

Three different solvation boundary conditions were used to help identify significant changes in dynamics upon drug binding. Water molecules defined in the X-ray structure determination represent those water molecules occupying a low-potential position. Other water molecules were added to model bulk solvent of the system by overlaying the energy-minimized X-ray coordinates with water molecules from a system equilibrated at bulk water density by molecular dynamics. Water molecules closer than 2.8 Å to crystallographic atoms are deleted. The equilibrated waters are overlayed multiple times; each overlay uses a unique combination of box translational and rotational coordinates to ensure complete system coverage. The three systems can differ not only in the number of water molecules arising from the above overlay procedure, but also by whether those water molecules are restrained by a boundary force (Brooks & Karplus, 1989). Solvation condition 1 has fewer water molecules than solvation condition 2 (or 3). Solvation conditions 1 and 2 have water molecules that are restrained by a boundary potential at 22 Å, while 3 has no solvent boundary potential. Conditions 2 and 3 have the same water overlays, thus equal number of water molecules. Finally, HRV14 and HRV14·WIN52084s differ in the number of water molecules (under each of the three solvation conditions) due to differences in the conformation of VP1.

The system consists of between 3,000 and 3,500 atoms, with a variable number of water molecules, WIN52084s (HRV14·WIN52084s simulations only), and 2,300 protein atoms. After overlaying with water the system was energy minimized and equilibrated

Table 3. *Temperature and total energy averaged over the 800 ps collection period*

	HRV14[a]		HRV14·WIN52084s[b]	
Solvation boundary	Temperature (K)	Total energy (kcal/mol)	Temperature (K)	Total energy (kcal/mol)
1 22 Å	297.2 ± 3.2	−10,882 ± 70	297.5 ± 3.2	−10,314 ± 72
2 22 Å	297.4 ± 3.0	−11,454 ± 67	296.1 ± 3.3	−10,478 ± 76
3 None	297.3 ± 2.9	−10,867 ± 73	296.8 ± 3.1	−10,364 ± 68

[a]Number of water molecules is 359, 416, and 416 for solvation boundary conditions 1, 2, and 3, respectively.
[b]Number of water molecules is 309, 375, and 375 for solvation boundary conditions 1, 2, and 3, respectively.

and heated by molecular dynamics for a period of 100 ps. The time step was 0.001 ps, and the target temperature was 300 K. The collection period was 800 ps.

To assess the stability of molecular dynamics simulations, it is useful to calculate simulation averages and trends. Average temperatures and total energies are given in Table 3. SBMD simulations mimic the coupling of a small system to a large heat bath, and the temperatures for the six simulations are nearly identical. In addition, the energies of these trajectories are quite similar. The somewhat lower energies of the HRV14 simulations likely arise from a greater number of water molecules. The stability of the simulations is further established by the small RMS difference of heavy atoms between coordinate snapshots of the trajectory and the energy-minimized X-ray coordinates (see Fig. 3). The constancy in RMS differences also indicates the absence of conformational drifts over the course of the simulation. The magnitude of the RMS differences is approximately the same for each of the six simulations and stabilizes around 1.9 to 2.0 Å, comparable to that found in other studies (Daggett & Levitt, 1993).

Results and discussion

Earlier work (Phelps & Post, 1995; Phelps et al., 1998) on HRV14 demonstrates how the hydrophobic properties of WIN52084s are reflected in density fluctuations (which can be used to calculate compressibility) and in the temperature dependence of mobility. Both properties appear to reflect the entropy of the system.

Fluctuation cross correlations

Binding of WIN52084s to HRV14 displaces several water molecules from the internal pocket, which leads to a replacement of

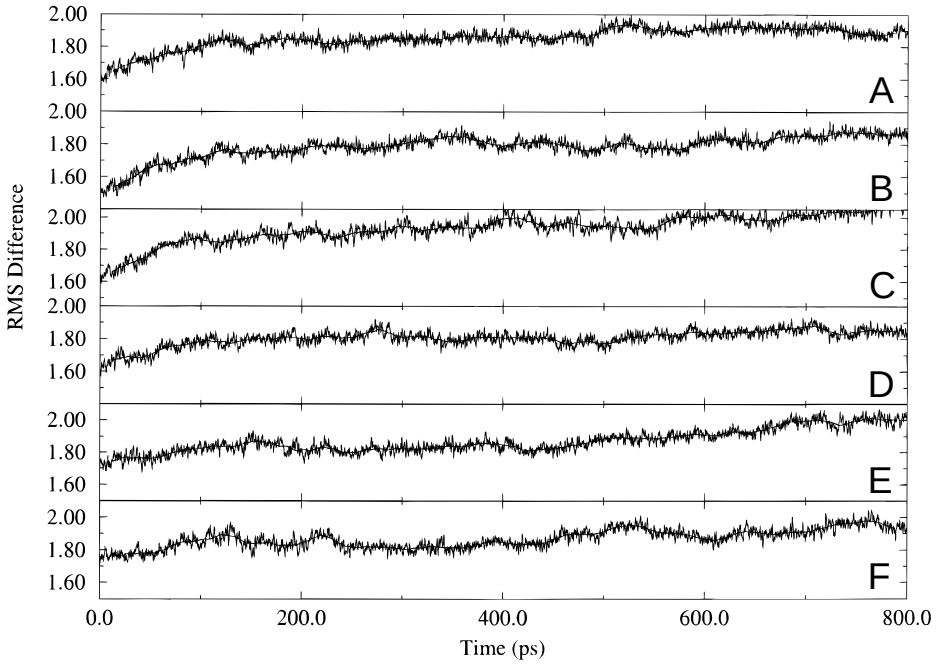

Fig. 3. RMS differences of all heavy atoms between coordinate snapshots during the collection period of the trajectory and energy-minimized X-ray coordinates. **A–C** and **D–F** represent solvation conditions 1–3 (see Table 3) for HRV14 and HRV14·WIN52084s, respectively.

polar interactions by hydrophobic ones. It is reasonable that changes in the nature of forces between atoms, whereby long-range polar or electrostatic forces are substituted by short-range hydrophobic (or van der Waals) forces, could cause changes in correlated motions. Therefore, cross-correlation coefficients, $C(i,j)$, in the fluctuations of atom i and j were calculated to evaluate the extent of positional correlation among atoms. When comparing HRV14 and HRV14·WIN52084s (results not shown), individual $C(i,j)$ values exhibit relatively small variations with no discernable trend. On the other hand, the dependence of the cross-correlation coefficients on the distance separating atom i and j did vary in the presence of the drug. The distance dependent correlation function $\overline{C(r)}$ can be calculated from the equations,

$$C(i,j) = \frac{\sum (\Delta r_i(t) \cdot \Delta r_j(t))}{\left[\sum \Delta r_i(t)^2\right]^{1/2}\left[\sum \Delta r_j(t)^2\right]^{1/2}}$$

$$\overline{C(r)} = \frac{\sum C(i,j|r)}{n(r(i,j))}$$

where $C(i,j)$ is the cross-correlation coefficient between atoms i and j, $\Delta r_i(t)$ is the distance between position of atom i at time t and its average position, $C(i,j|r)$ is the cross-correlation coefficient for an atom separated by the distance r, and $n(r)$ is the number of (i,j) pairs separated by distance r.

$\overline{C(r)}$ calculated for HRV14 and HRV14·WIN52084s were least-squares fit with excellent agreement to the empirical equation $\overline{C(r)} = A\exp(-r/r_c)$ (see Table 4). The form of this equation gives r_c as a "correlation length." The greater the value of r_c, the larger the length over which atoms show correlated motion. Comparison of HRV14 and HRV14·WIN52084s under the same solvation boundary conditions show larger correlation lengths, r_c, for HRV14. The respective value of r_c for the three conditions for unligated HRV14 is 8.0, 7.3, and 9.9 Å, while correlated motions fall off at 6.1, 6.6, and 7.2 Å, respectively, for HRV14·WIN52084s. Again, this behavior is consistent with earlier arguments (Phelps & Post, 1995; Phelps et al., 1998) that weaker interatomic interactions occur with pocket-bound WIN52084s and argues against structural rigidification as the mechanism of antiviral activity.

An earlier study of cross correlations in bovine pancreatic trypsin inhibitor (Ichiye & Karplus, 1991) found that the behavior was more complicated than a simple exponential decay. They report an initial decay in cross correlation as a function of distance between atoms, followed by a small increase at distances corresponding to molecular size. In the cases reported here, the correlations decay exponentially to zero over distances of 30 Å without an increase at long distances. It is not clear whether the different behavior in long-range cross correlations is due to the lack of a full molecular system with the SBMD method or some other factor.

Table 4. *Fit of distance dependent correlation function* $\overline{C(r)}$ *to the empirical function* $A\exp(-r/r_c)$

	HRV14			HRV14·WIN52084s		
Solvation boundary	A	r_c (Å)	Correlation coefficient	A	r_c (Å)	Correlation coefficient
1	0.592	7.98	−0.981	0.981	6.10	−0.990
2	0.664	7.29	−0.992	0.975	6.58	−0.988
3	0.659	9.93	−0.990	0.777	7.24	−0.993

Positional fluctuations

A second approach for assessing the motions of proteins is in RMS positional fluctuation build-up curves (Post et al., 1989). Points in these curves are obtained by calculating the RMS positional fluctuations for a given time interval and averaging over all distinct time intervals of this length. Consequently, from an 800 ps trajectory, one datum determines the 800 ps value, while the 400 ps value is the average of two data points. Structural elements constrained to a small portion of configuration space have build-up curves that smoothly and monotonically increase to a limiting value. The smaller the accessible configuration space the more quickly a limiting value will be reached. Conversely, if a large space is accessible, then a longer time is needed to plateau. If there is a structural transition between energy minima, then there will be a discontinuous increase in the curve when the time interval is sufficiently long for the system to sample both minima.

The most important structural elements present in the simulations are the BIDG and CHEF β-sheets of VP1 (see Fig. 1). Short fragments of α-helices and other β-strands are within the SBMD sphere; however, these structures consist largely of harmonically constrained atoms near the edge of the sphere. The RMS positional fluctuation build-up curves for BIDG and CHEF β-sheets of VP1 are given in Figure 4. The overall fluctuations are relatively small as expected for β-sheets (McCammon & Harvey, 1987; Post et al., 1989).

Most striking is the behavior seen for the C-strand (solid curve) of the CHEF sheet shown in the right column. For both HRV14 (A–C) and HRV14·WIN52084s (D–F), the C-strand is consistently more mobile than other strands of the sheet. In addition, the H-strand (dotted curve) is generally higher than E- or F-strands. The distinction of the C-strand behavior from that of the others is unusual. In other studies and for the BIDG sheet in five of the six viral simulations, all strands in a sheet have similar build-up curves (Post et al., 1989), consistent with a collective motion of the entire β-sheet. The proximity of the C-strand to the viral exterior and its relatively high mobility suggest that it may provide an entry point to the drug-binding pocket. The putative pocket entrance interpreted by Rossmann and coworkers by visual inspection of the structure is this region of VP1 including the C-strand.

Neither the CHEF nor BIDG build-up curves distinguish HRV14 and HRV14·WIN52084s consistently under all solvation boundary conditions. Thus, the presence of a drug does not alter these picosecond–time-scale fluctuations.

The 800 ps RMS fluctuations were compared to B-values from the X-ray structure determinations by the equation: $\langle \Delta R^2 \rangle^{1/2} = [(3/8\pi^2)B]^{1/2}$ where B is the crystallographic B-value and $\langle \Delta R^2 \rangle^{1/2}$ are RMS fluctuations. RMS fluctuations for the six simulations and converted B-values for HRV14 main-chain atoms are compared in Figure 5. We note that crystallographic B-values are not available for HRV14·WIN52084s. Harmonically constrained residues are highlighted by yellow bands and show a variety of behavior; fluctuations are neither uniformly large nor small, and the range of fluctuations is similar to that observed for residues in the unconstrained MD portion of the SBMD sphere. Thus, the use of SBMD does not appear to unduly restrict the motion of boundary

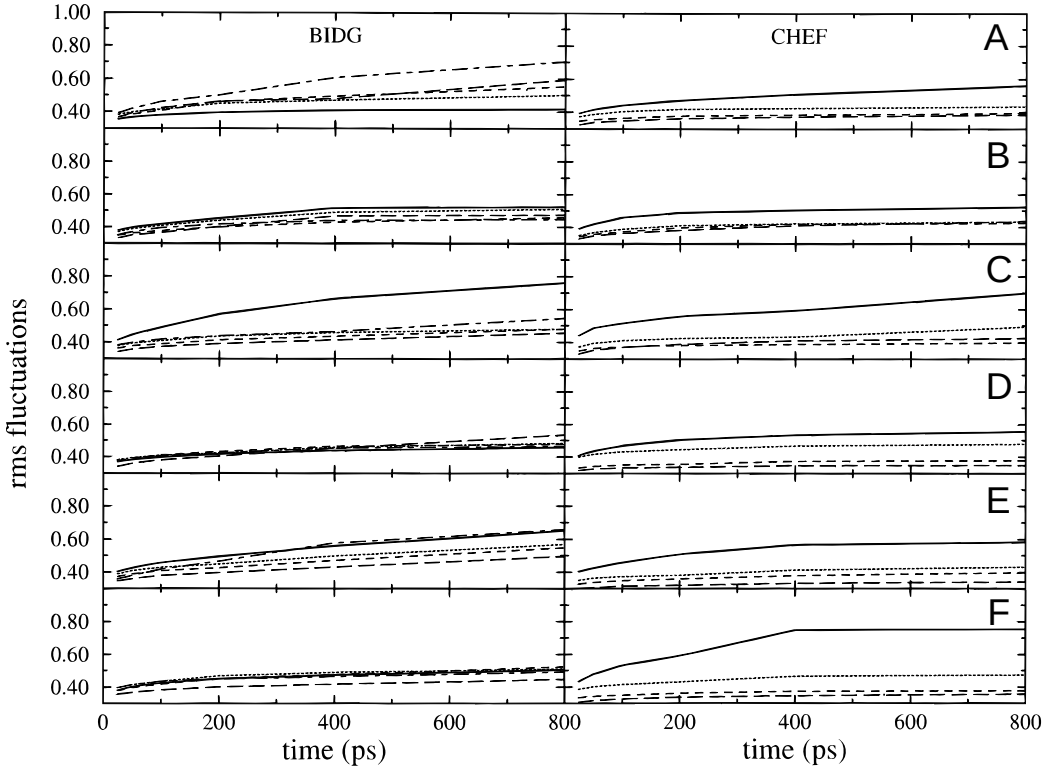

Fig. 4. RMS fluctuations of main-chain atomic positions as a function of averaging period. **A–C** and **D–F** represent solvation conditions 1–3 (see Table 3) for HRV14 and HRV14·WIN52084s, respectively. Left column shows build-up curves for strands of the BIDG β-sheet with solid line = strand B; dotted line = strand I; short dash = strand D; long dash = strand G_1; dot-dash = strand G_2. Right column has CHEF β-sheet strands with solid line = strand C; dotted line = H strand; short dash = E strand; long dash = F strand.

atoms. The simulations have RMS fluctuations quite similar in magnitude to those estimated from *B*-values for the HRV14 X-ray structure. The *B*-values show less variation with residue that may reflect the refinement procedure rather than the actual thermal motion. Alternatively, limited sampling over the 800 ps period of the simulation would give the greater variations seen in panels A–F relative to panel G.

Although the residue profiles for positional fluctuations vary among the six simulations, some general trends are found in Figure 5. The β-strand RMS fluctuations for BIDG and CHEF sheets (highlighted by gray bands) are generally low and similar to one another, as noted above in the discussion of build-up curves, while the loop regions (white bands) have larger fluctuations overall. The FMDV loop displays considerable flexibility in X-ray data, flexibility that is also evident in the simulation results. Similarly, the loop between βE and αB has significant mobility according to X-ray *B*-values, and this motion is also identified by the simulations.

In particular, large RMS fluctuations compared to most other residues, are found for VP4 from both the X-ray data and the simulation results. The motions of VP4 may be particularly relevant to viral dissassembly (Grant et al., 1994). VP4 lies on the inner surface of the viral protein capsid and is believed to exit the virus interior at an early stage of dissassembly.

Examination of Figure 5 finds no consistent change in fluctuations as a result of drug binding. The statistical differences among the six simulations is more evident than any consistent distinction between the top curves A–C and the bottom curves D–F. This lack of distinction in individual atomic fluctuations in the presence of the drug is in contrast to the consistent effect of WIN on the larger scale properties $\overline{C(r)}$ and compressibility (Phelps & Post, 1995).

Interaction energies

The significant changes in the conformational properties of HRV14 and HRV14·WIN52084s have been linked to the substitution of polar interactions from water molecules in the drug-binding pocket for the hydrophobic interactions of WIN52084s (Phelps & Post, 1995; Phelps et al., 1998). This exchange of polar for apolar interactions can be examined by calculating the interaction energies between protein atoms from residues lining the drug-binding pocket (pocket residues) and atoms in molecules occupying the pocket: WIN52084s and pocket water molecules. Pocket water molecules are specifically those molecules inside the drug-binding pocket of VP1. The pocket residues are defined to be those residues having an atom within 5.0 Å of the centers of any WIN atom in the X-ray energy minimized structure. The time-averaged intermolecular interaction energies are broken down into van der Waal and electrostatic components in Table 5. Under each of the three solvation boundary conditions, the interactions between pocket residue atoms and molecules occupying the pocket are more nonpolar in nature (stronger van der Waals and weaker electrostatic energy) for HRV14·WIN52084s than for HRV14, yet the total intermolecular interaction energy is weaker in HRV14·WIN52084s. That this one component of a binding enthalpy does not favor drug binding supports the earlier conclusion that the experimentally determined stabilization by the drug (Fox et al., 1986; Rombaut et al., 1991;

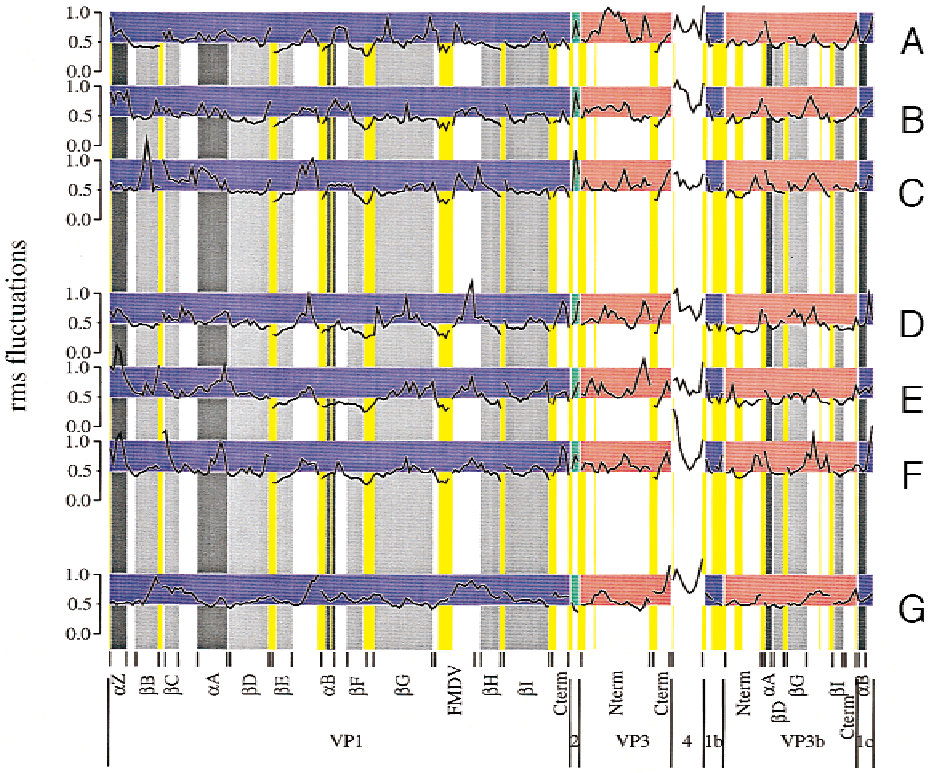

Fig. 5. RMS fluctuations of main-chain atoms over 800 ps trajectory period shown by residue. **A–C** and **D–F** represent solvation conditions 1–3 for HRV14 and HRV14·WIN52084s, respectively. Panel **G** has HRV14 crystallographic *B*-values rescaled to RMS fluctuations by the equation: $\langle \Delta R^2 \rangle^{1/2} = [(3/8\pi^2)B]^{1/2}$. The 235 residues in these simulations are VP1: 67–82, 99–132, 147–161, 166–205, 213–228, 240–254, 264–269; VP2: 205–207; VP3: 13–34,231–236; VP4: 32–41; VP1b: 63–65, 72–74; VP3b: 7–18, 102–108, 170–183, 218–225; VP1c: 168–172.

Bibler-Muckelbauer et al., 1994) is entropically based. The intramolecular interaction energies involving pocket and the protein atoms further from the drug, or the nonpocket protein atoms, are also shown in Table 5. These interactions have similar van der Waal and electrostatic energy values whether for unligated HRV14 or ligated HRV14·WIN52084s.

More globally, increases in compressibility upon drug binding should be a reflection of changes in interaction energies not only between pocket and nonpocket atoms, but between HRV14 protein subunits. Accordingly, the system was apportioned between the various viral proteins indicated in Figure 5, VP1, VP3, VP4, and VP3b (VP3b is from a different symmetry related protomeric unit than VP3), WIN52084s, and pocket waters. The interaction energies tabulated in Table 6 are the sums of the van der Waal and electrostatic terms between two portions of the system on a basis of per-unit surface contact area. Such normalization to contact area

Table 5. *Time-averaged van der Waals and electrostatic energies per pocket residue of the HRV14 binding pocket*

Interacting groups	Solvation boundary	HRV14 (kcal/mol)		HRV14·WIN52084s (kcal/mol)	
		van der Waals	Electrostatic	van der Waals	Electrostatic
Pocket residue[a] H_2O + WIN52084s	1	−3.0	−9.6	−4.3	−6.9
	2	−3.2	−15.9	−4.1	−11.7
	3	−5.0	−12.2	−3.3	−7.9
Pocket residue nonpocket protein[b]	1	−13.4	−21.8	−13.1	−20.6
	2	−13.3	−17.9	−13.2	−16.1
	3	−13.9	−18.9	−12.7	−17.1

[a] Protein residues lining the binding pocket of HRV14 are residues that have any atom within 5 Å of any WIN52084s atom defined by the crystallographic coordinates following energy minimization. This list is not varied over the course of the simulations for the time averaging.

[b] Protein residues not lining the binding pocket of HRV14.

Table 6. *Time-averaged interaction energies per Å^2 of surface contact area between individual viral proteins and either other protein, WIN52084s, or pocket water molecules*

Interacting groups	Solvation boundary	Interaction energies (kcal/mol/Å^2)[a]		
		HRV14	HRV14·WIN52084s	HRV14·pWIN52084s
VP1[b] protein	1	−1.37	−1.37	
	2	−1.37	−1.36	−1.36
	3	−1.37	−1.36	−1.36
VP1 WIN52084s	1		−0.34	
	2		−0.34	−0.38
	3		−0.34	−0.38
VP1 pocket waters	1	−0.57	−0.11	
	2	−0.66	−0.10	−0.10
	3	−0.65	−0.11	−0.10
VP3[c] protein	1	−1.50	−1.54	
	2	−1.48	−1.54	−1.54
	3	−1.47	−1.54	−1.54
VP3 WIN52084s	1		−0.01	
	2		−0.01	−0.01
	3		−0.01	−0.01
VP3b[d] protein	1	−0.89	−0.89	
	2	−0.88	−0.89	−0.89
	3	−0.88	−0.89	−0.89
VP3b WIN52084s	1		0.0	
	2		0.0	0.0
	3		0.0	0.0
VP4[e] protein	1	−1.40	−1.43	
	2	−1.37	−1.44	−1.43
	3	−1.37	−1.43	−1.43
VP4 WIN52084s	1		0.0	
	2		0.0	0.0
	3		0.0	0.0

[a] Surface area is calculated with method of Lee and Richard using the minimized X-ray coordinates and a probe radius equal to 0.0 Å.
[b] 142 residues, contact surface area = 692 Å^2.
[c] 28 residues, contact surface area = 432 Å^2.
[d] 41 residues, contact surface area = 462 Å^2.
[e] 10 residues, contact surface area = 134 Å^2.

was made to more reasonably compare the energies when significant differences occur in the number of residues in each group.

The difference in the polarity of the atomic interactions for the free and drug-bound states of the viral proteins noted from the spatial partitioning of interacting atoms (Table 5) is also apparent from the molecular partitioning (Table 6). That is, intermolecular interaction energies for VP1, the viral protein forming the binding pocket, are collectively somewhat less favorable for HRV14·WIN52084s ($-0.10 + -0.34$ kcal/mol/Å^2) or HRV14·pWIN52084s ($-0.10 + -0.38$ kcal/mol/Å^2) than for HRV14 (-0.60 kcal/mol/Å^2).

Of particular interest regarding the values in Table 6 is the smaller VP3b *inter*-protomeric interaction energies; the interactions of VP3b with other protein is -0.9 kcal/mol/Å^2, significantly less favorable than the value of -1.4 to -1.5 kcal/mol/Å^2 calculated for subunit interactions involving VP1, VP3, or VP4, and largely within one protomeric unit. The stronger *intra*-protomeric associations relative to interprotomeric ones was noted earlier with respect to total dimer associations (Reddy et al., 1998) and may be significant for assembly. To our knowledge, the more favorable interaction on a per unit contact area has not been recognized.

Conclusions

The native HRV14 drug-binding pocket contains eight water molecules; most are displaced by the hydrophobic WIN52084s upon drug binding. This exchange of polar for apolar interactions is reflected in larger scale, collective motions of the protein that differ in behavior between HRV14 and HRV14·WIN52084s. In this paper, we have shown from the distance dependence of the cross correlations between atomic fluctuations that the correlation length is longer for HRV14 than HRV14·WIN52084s, reflecting a greater influence of long-range polar interactions in HRV14. This behavior is evidence that the drug does not act by a mechanism of structural rigidification, but rather by making a more conformationally supple system with higher entropy. Recent experiments

show remarkable evidence for large, transient conformational fluctuations in unligated HRV14 based on the sensitivity to proteolytic cleavage of residues in VP1 and VP4, which are not readily accessible (Lewis et al., 1998). Moreover, these large amplitude fluctuations appear to be significantly damped by a WIN compound because the protease does not cleave these residues in the presence of drug. The shorter correlation length motions in $\overline{C(r)}$ (Table 4) are consistent with this effect of binding WIN compounds.

The modification to the interatomic interactions by drug binding is fully consistent with previous conclusions. In our earlier work (Phelps & Post, 1995) HRV14·WIN52084s was found to have larger density fluctuations and hence greater compressibility than HRV14; the estimated compressibility of 12.1×10^{-6} bar^{-1} for HRV14·WIN52084s is greater than that of 8.8×10^{-6} bar^{-1} for HRV14. (Values are the average of compressibilities given in Table 1 of Phelps & Post, 1995.) This greater compressibility can be used to roughly estimate (estimated from compressibilities in Table 1 and entropies calculated from the regression line in Fig. 4 of Phelps & Post, 1995) a stabilizing entropy of 1.1–2.6 J/K/(mol-residue) for HRV14·WIN52084s over HRV14. In addition, molecular dynamics studies at different temperatures (Phelps et al., 1998) found a significant shift in the temperature dependent mobility of these two systems. In each case, the differences can be traced to weaker, less polar interatomic forces in the drug-binding pocket.

Fast time-scale properties, such as picosecond fluctuation magnitudes and their time development, do not reflect drug function; these properties varied as much among the three simulations with different solvation boundary conditions as differences between unligated and drug-bound HRV14 simulations. In contrast, insight into the mechanism of antiviral activity is gained from considering the larger scale properties: distance-dependent cross correlations, density fluctuations/compressibility, and temperature dependent mobility.

We have also described interaction energies of various viral proteins with WIN52084s and pocket water molecules that reflect the changes in intermolecular interactions associated with the pocket. Water molecules alone are energetically more favorable and more polar in nature than the combined interactions of pocket water molecules and WIN52084s. Accordingly, the experimentally observed increase in thermal stability is reasonably based on entropic effects rather than enthalpic ones.

Analysis of the simulation results also identified structural features related to drug binding and viral assembly that can be tested experimentally by amino acid mutation or other means. Larger fluctuation magnitudes in the C-strand of the CHEF β-sheet of VP1 suggest a potential drug entry site that is fully consistent with what appears visually to be the pocket opening (Kim et al., 1993). Second, intersubunit interactions for subunits within a viral protomer were found to be stronger compared to subunit contact energy between protomers, which is likely important for directing capsid assembly.

Acknowledgments

This work was supported by NIH Grant AI39639 to C.B.P. and the Lucille P. Markey Foundation.

References

Bibler-Muckelbauer JK, Kremer MJ, Rossmann MG, Diana GD, Dutko FJ, Pevear DC, McKinlay MA. 1994. Human rhinovirus 14 complexed with fragments of active antiviral compounds. *Virology 202*:360–369.

Brooks BR, Bruccoleri RE, Olafson BD, States DJ, Swaminathan S, Karplus M. 1983. CHARMM: A program for macromolecular energy, minimization and dynamics calculations. *J Comput Chem 4*:187–217.

Brooks CI, Karplus M. 1983. Deformable stochastic boundaries in molecular dynamics. *J Chem Phys 79*:6312–6325.

Brooks CL III, Karplus M. 1989. Solvent effects on protein motion and protein effects on solvent motion: Dynamics of the active site region of lysozyme. *J Mol Biol 208*:159–181.

Daggett V, Levitt M. 1993. Realistic simulations of native-protein dynamics in solution and beyond. *Annu Rev Biophys Biomol Struct 22*:353–380.

Filman DJ, Syed R, Chow M, Macadam AJ, Minor PD, Hogle JM. 1989. Structural factors that control conformational transitions and serotype specificity in type 3 poliovirus. *EMBO J 8*:1567–1579.

Fox M, Otto M, McKinlay M. 1986. The prevention of rhinovirus and poliovirus uncoating by WIN51711: A new antiviral drug. *Antimicrob Agents Chemother 30*:110–116.

Grant RA, Hiremath CN, Filman DJ, Syed R, Andries K, Hogle JM. 1994. Structures of poliovirus complexes with antiviral drugs: Implications for viral stability and drug design. *Curr Biol 4*:784–797.

Heinz B, Shepard D, Rueckert R. 1990. Escape mutant analysis of a drug-binding site can be used to map functions in the rhinovirus capsid. In Laver W, Air G, eds. *Use of X-ray crystallography in the design of antiviral agents*. San Diego: Academic Press. pp 173–186.

Ichiye T, Karplus M. 1991. Collective motions of proteins: A covariance analysis of atomic fluctuations in molecular dynamics and normal mode simulations. *Proteins Struct Funct Genet 11*:205–217.

Kim K, Willingmann P, Gong Z, Kremer M, Chapman M, Minor I, Oliveira M, Rossmann M, Andries K, Diana G, et al. 1993. A comparison of the anti-rhinoviral drug binding pocket in HRV14 and HRV1a. *J Mol Biol 230*:206–226.

Kraulis P. 1991. MOLSCRIPT: A program to produce both detailed and schematic plots of protein structures. *J Appl Crystallogr 24*:946–950.

Lewis J, Bothner B, Smith T, Siuzdak G. 1998. Antiviral agent blocks breathing of the common cold virus. *Proc Natl Acad Sci USA 95*:6774–6778.

Lybrand T, McCammon J. 1988. Computer simulation study of the binding of an antiviral agent to a sensitive and a resistant human rhinovirus. *J Comput Aided Mol Des 2*:259–266.

McCammon JA, Harvey SC. 1987. *Dynamics of proteins and nucleic acids*. Cambridge, UK: Cambridge University Press.

Merritt E, Bacon D. 1997. Raster3d photorealistic molecular graphics. *Methods Enzymol 277*:505–524.

Phelps D, Post C. 1995. A novel basis for capsid stabilization by antiviral compounds. *J Mol Biol 254*:544–551.

Phelps D, Rossky P, Post C. 1998. Influence of an antiviral compound on the temperature dependence of viral protein flexibility and packing: A molecular dynamics study. *J Mol Biol 276*:331–337.

Post CB, Dobson CM, Karplus M. 1989. A molecular dynamics analysis of protein structural elements. *Proteins 5*:337–354.

Reddy V, Giesgin H, Morton R, Kuman A, Post C, Brooks C, Johnson J. 1998. Energetics of quasiequivalence: Computational analysis of protein–protein interactions in icosahedral viruses. *Biophys J 74*:546–558.

Rombaut B, Andries K, Boeye A. 1991. A comparison of WIN51711 and R78206 as stabilizers of poliovirus virions and procapsids. *J Gen Virol 72*:2153–2157.

Rossmann M. 1994. Viral cell recognition and entry. *Protein Sci 3*:1712–1725.

Rossmann M, Arnold E, Erickson J, Frankenberger E, Griffith J, Hecht J, Johnson J, Kamer G, Luo M, Mosser A, et al. 1985. Structure of a human cold virus and functional relationship to other picornaviruses. *Nature 317*:145–153.

Ryckaert JP, Ciccotti G, Berendsen HJC. 1977. Numerical integration of the cartesian equations of motion of a system with constraints: Molecular dynamics of *n*-alkanes. *J Comp Phys 23*:327–341.

Smith T, Kremer M, Luo M, Vriend G, Arnold E, Kamer G, Rossmann M, McKinlay M, Diana G, Otto M. 1986. The site of attachment of human rhinovirus 14 for antiviral agents that inhibit uncoating. *Science 233*:1286–1293.